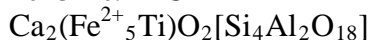


**2013-109**  
**KURATITE**

**CONFIDENTIAL INFORMATION**

DEADLINE: 30 NOVEMBER 2013

**2013-109 KURATITE**



Triclinic                      Space group:  $P\bar{1}$  (by analogy to rhönite)  
 $a = 10.513 \pm 0.007$        $b = 10.887 \pm 0.007$                        $c = 9.004 \pm 0.018 \text{ \AA}$   
 $\alpha = 105.97 \pm 0.13$        $\beta = 96.00 \pm 0.12$                        $\gamma = 124.82 \pm 0.04^\circ$   
 $V = 767 \pm 2 \text{ \AA}^3$                        $Z = 2$

Shyh-Lung Hwang<sup>1\*</sup>, Pouyan Shen<sup>2</sup>, Hao-Tsu Chu<sup>3</sup>, Tzen-Fu Yui<sup>4</sup>, Maria-Eugenia Varela<sup>5</sup> and Yoshiyuki Iizuka<sup>4</sup>

<sup>1</sup>Department of Materials Science and Engineering, National Dong Hwa University, Hualien, Taiwan, ROC

<sup>2</sup>Institute of Materials Science and Engineering, National Sun Yat-sen University, Kaohsiung, Taiwan, ROC

<sup>3</sup>Central Geological Survey, PO Box 968, Taipei, Taiwan, ROC

<sup>4</sup>Institute of Earth Sciences, Academia Sinica, Taipei, Taiwan, ROC

<sup>5</sup>Instituto de Ciencias Astronómicas de la Tierra y del Espacio (ICATE) Avenida España 1512 sur, J5402DSP, San Juan, Argentina

\*E-mail: [slhwang@mail.ndhu.edu.tw](mailto:slhwang@mail.ndhu.edu.tw)

**OCCURRENCE**

The mineral occurs in the D'Orbigny angrite, a 16.5 kg meteorite found in July 1979 in Argentina. The polished angrite slab sample *ca* 1.5 x 1.5 x 0.3 cm in size used for the present study was kindly loaned by the Naturhistorisches Museum Wien, Austria (inventory number: Section D'Orbigny C-N1172-NH Wien). Detailed petrographic descriptions of the D'Orbigny angrite are available (Mittlefehldt *et al.*, 2002; Kurat *et al.*, 2004; Varela *et al.*, 2003). See Authors' Remarks.

Associated minerals are olivine intergrowths with Ca-rich fayalite (Ca ~20 mol%) + kirschsteinite (Ca ~40 mol%), Fe sulfides, ulvöspinel, Na-bearing anorthite, whitlockite and Al-bearing hedenbergite (Figure 1a, b) as multiple phase pockets sitting at grain triple junctions of olivine (with rims of Fe/Ca-rich olivine overgrowths) + augite (with rims of hedenbergite) aggregates.

The mineral formed as a primary phase (see Authors' Remarks).

**APPEARANCE and PHYSICAL PROPERTIES**

Kuratite crystals typically are euhedral to anhedral in shape, < 20  $\mu\text{m}$  in size, and occur, along with whitlockite and submicrometer-sized Fe sulfide droplets, within a rim of olivine with Ca-rich fayalite composition (Ca ~20 mol%) + kirschsteinite (Ca ~40 mol%) intergrowths at the contact between Fe sulfide spherules and the space-filling hedenbergite (Figure 1c-e). Such intergrowths were not observed between Fe sulfide spherules and the olivine overgrowth rim enriched with Fe/Ca (Figure 1f). Whitlockite inclusions in kuratite are frequently observed (Figure 1d, e).

Physical properties are not available, because of the minute size of the kuratite crystals in the sample. Data for rhönite (Anthony *et al.*, 1995), where appropriate, are given below.

Colour: dark brown to black (rhönite)

**2013-109**  
**KURATITE**

Lustre: semimetallic (rhönite)

H (Mohs): 5-6 (rhönite)

Cleavage: {010}, {001} good (rhönite); rhönite with  $Mg^{2+}/(Mg^{2+}+Fe^{2+}) = 0.46$  has no discernible cleavage (Olsson, 1983)

Density could not be measured because of small grain size

Density (calc.) =  $3.937 \text{ g cm}^{-3}$  using the empirical formula

No additional physical properties were reported by the authors listed by Grew *et al.* (2008).

### OTHER PROPERTIES

The Raman spectrum of kuratite shows four main scattering peaks near 563-571, 697-699 (strongest), 852-856 and 986-996  $\text{cm}^{-1}$  resembling that of lunar rhönite (Treiman, 2008) but with higher frequencies due to different chemical composition (Figure 2). A weak shoulder on the strongest peak at 720  $\text{cm}^{-1}$  was recognized in lunar rhönite (Treiman, 2008) but not kuratite.

### OPTICAL PROPERTIES

Optical properties are not available because of the minute size of the kuratite crystal sample and the nearly opaque nature of the multiple-phase pockets of mesostasis phases according to OM observations.

Rhönite is biaxial (+), strongly pleochroic and exhibits extreme dispersion (Anthony *et al.*, 1995)

$Fe^{2+}$ -dominant rhönite ( $X_{Mg} = 0.02-0.5$ ) is biaxial (+), red brown or yellow brown in thin section ( $< 15 \mu\text{m}$ ). It exhibits strong pleochroism from greenish brown (X) to dark reddish brown (Z). Other data available from the literature are  $n_x = 1.805 \pm 0.007$ ,  $n_y = 1.815 \pm 0.007$ ,  $n_z = 1.845 \pm 0.007$ ,  $2V = 50 \pm 3^\circ$  for Puy de St.-Sandoux rhönite ( $X_{Mg} = 0.49$ );  $Z \wedge c = 38-43^\circ$  for Kaiserstuhl rhönite ( $X_{Mg} = 0.41$ );  $Z \wedge c = 58^\circ$  ( $X_{Mg} = 0.02$ ) for Luna 24 rhönite (Grapes and Keller, 2010; Grünhagen and Seek, 1972; Olsson, 1983; Treiman, 2008).

### CHEMICAL DATA

Chemical analyses (8 analyses from 4 different grains) were carried out using a JEOL JXA8500-F FE-electron microprobe (WDS mode, 12 kV, 5 nA, 2  $\mu\text{m}$  beam diameter). Analytical data are given in Table 1.

Table 1. Analytical data for kuratite.

	B5-a-3	B5-a-4	B5-a-5	B5-a-6	B5-a-7	B5-a-8	B5-a-9	B5-a-10	Average
SiO <sub>2</sub>	25.37	25.16	25.95	25.06	26.39	25.21	25.50	25.80	25.55
TiO <sub>2</sub>	8.43	9.17	8.52	8.51	9.78	8.68	8.33	8.15	8.70
Al <sub>2</sub> O <sub>3</sub>	10.32	10.18	9.53	9.35	8.86	10.29	10.01	9.90	9.80
Cr <sub>2</sub> O <sub>3</sub>	0.00	0.00	0.00	0.00	0.00	0.00	0.11	0.00	0.01
Y <sub>2</sub> O <sub>3</sub>	0.08	0.00	0.05	0.04	0.03	0.00	0.00	0.00	0.03
La <sub>2</sub> O <sub>3</sub>	0.23	0.00	0.00	0.00	0.00	0.00	0.03	0.07	0.04
Pr <sub>2</sub> O <sub>3</sub>	0.15	0.00	0.22	0.00	0.18	0.12	0.06	0.00	0.09
Nd <sub>2</sub> O <sub>3</sub>	0.18	0.01	0.00	0.00	0.13	0.21	0.00	0.00	0.07
FeO	42.01	41.09	40.98	41.76	41.95	41.86	41.60	41.57	41.60
MnO	0.20	0.02	0.04	0.13	0.06	0.03	0.24	0.15	0.11
NiO	0.01	0.00	0.15	0.00	0.00	0.19	0.00	0.18	0.07
SrO	0.06	0.08	0.04	0.04	0.05	0.03	0.00	0.06	0.05
ZnO	0.00	0.00	0.00	0.00	0.22	0.00	0.03	0.10	0.04
MgO	0.00	0.02	0.00	0.06	0.00	0.02	0.00	0.01	0.01

**2013-109**  
**KURATITE**

CaO	11.92	11.86	11.84	11.78	11.56	12.10	11.96	11.82	11.86
Na <sub>2</sub> O	0.00	0.02	0.13	0.03	0.01	0.00	0.07	0.04	0.04
K <sub>2</sub> O	0.01	0.00	0.00	0.00	0.00	0.01	0.00	0.01	0.00
P <sub>2</sub> O <sub>5</sub>	0.27	0.16	0.20	0.23	0.08	0.17	0.19	0.27	0.20
F	0.00	0.00	0.00	0.00	0.00	0.02	0.03	0.00	0.01
Cl	0.03	0.00	0.02	0.04	0.03	0.04	0.00	0.01	0.02
SO <sub>3</sub>	0.09	0.07	0.06	0.13	0.08	0.05	0.09	0.05	0.08
Total									98.38

The empirical formula (based on 20 O *apfu*) is (with grouping; other grouping is possible)  $(\text{Ca}_{1.95}\text{Na}_{0.01}\text{REE}^{3+}_{0.01}\text{Mn}_{0.01}\text{Ni}_{0.01}\text{Zn}_{0.01})_{\Sigma 2.00}(\text{Fe}_{5.35}\text{Ti}_{0.72})_{\Sigma 6.07}(\text{Si}_{3.93}\text{Al}_{1.78}\text{Ti}_{0.29}\text{P}_{0.03}\text{S}_{0.01})_{\Sigma 6.04}\text{O}_{20}\text{F}_{0.01}\text{Cl}_{0.01}$ . Ignoring S, P, F, Cl as impurities gives  $(\text{Ca}_{1.95}\text{Na}_{0.01}\text{REE}^{3+}_{0.01}\text{Mn}_{0.01}\text{Ni}_{0.01}\text{Zn}_{0.01})_{\Sigma 2.00}(\text{Fe}_{5.35}\text{Ti}_{0.72})_{\Sigma 6.07}(\text{Si}_{3.93}\text{Al}_{1.78}\text{Ti}_{0.29})_{\Sigma 6.00}\text{O}_{20}$ .

The simplified formula is  $\text{Ca}_2(\text{Fe}^{2+}_5\text{Ti})(\text{Si}_4\text{Al}_2)\text{O}_{20}$  or, following the nomenclature scheme of Grew *et al.* (2008),  $\text{Ca}_4(\text{Fe}^{+2}_{10}\text{Ti}_2)\text{O}_4[\text{Si}_8\text{Al}_4\text{O}_{36}]$ .

### CRYSTALLOGRAPHY

For the purpose of determining the unit cell parameters of kuratite by electron crystallography, two TEM thin sections were prepared by the FIB technique (inserts in Figure 1d, e). The TEM bright-field images of these two FIB sections are given in Figure 3. Single-crystal X-ray studies were carried out using electron diffraction. Selected area electron diffraction (SAED) patterns were obtained from micrometer-sized kuratite crystals using a JEOL 3010 AEM. For each diffraction pattern, only 2 or 3 of the shortest nonlinear reciprocal vectors were measured for *d* spacing calculations. In general, the largest *d* spacing among a row of reflections with multiple *hkl* was used for unit cell refinement. The error of the *d* spacing measurements on SAED patterns taken at a camera length of 120 cm and calibrated by Al standard was estimated to be  $\pm 0.002$  nm. Unit cell parameters were refined from measured *d* spacings on electron diffraction patterns (Table 2).

Based on the least-squares refinement of 24 *d* spacings (Table 2) measured from SAED patterns of eleven zone axes, including the eight shown in Figure 4 ( $[11\bar{3}]$ ,  $[00\bar{1}]$ ,  $[0\bar{1}\bar{1}]$ ,  $[0\bar{1}\bar{4}]$ ,  $[\bar{1}\bar{1}\bar{2}]$ ,  $[\bar{1}\bar{2}\bar{2}]$ ,  $[\bar{1}\bar{1}\bar{3}]$ ,  $[\bar{1}\bar{1}\bar{4}]$ ) and three not shown ( $[0\bar{1}\bar{3}]$ ,  $[0\bar{1}\bar{2}]$ ,  $[10\bar{2}]$ ), from the twin-free kuratite crystal in section FIB-2, cell parameters of kuratite are very similar to those of other rhönite group minerals (Table 3). In comparison to rhönite with abundant  $\text{Mg}^{2+}$  (Table 3), the slightly larger unit cell parameters of kuratite must be due to the  $\text{Fe}^{2+}$  replacing  $\text{Mg}^{2+}$  in the octahedral site. Note that double-diffraction effects in electron diffraction usually alters intensity differences between spots, and therefore prohibits quantitative determination of the relative intensities among the reflections. This is especially true for the low-order zone patterns such as  $[00\bar{1}]$ ,  $[0\bar{1}\bar{1}]$ ,  $[\bar{1}\bar{1}\bar{2}]$  and  $[\bar{1}\bar{2}\bar{2}]$ , in which many reflections are present and double-diffraction effects prevail. However, for the high-order zone patterns with fewer reflections, the strong reflections can still be ascertained, such as  $\bar{2}\bar{1}\bar{1}$  and  $\bar{4}\bar{1}\bar{1}$  in the  $[11\bar{3}]$  zone,  $2\bar{2}\bar{1}$  in the  $[\bar{1}\bar{1}\bar{4}]$  zone,  $0\bar{3}\bar{1}$  and  $\bar{2}\bar{5}\bar{1}$  in the  $[\bar{1}\bar{1}\bar{3}]$  zone, as well as  $\bar{2}\bar{4}\bar{1}$  in the  $[0\bar{1}\bar{4}]$  zone (Figure 4). Although the  $4\bar{2}0$  reflection does not appear to be very strong in the  $[\bar{1}\bar{2}\bar{2}]$  zone of section FIB-2 (Figure 4f) due to double diffraction, it is in fact one of the strongest reflections for aenigmatite-rhönite group minerals and appears to be so in the  $[364]$  and  $[362]$  zone-axis patterns from section FIB-1, as shown in Figure 5. Additional strong reflections  $20\bar{3}$  and  $21\bar{3}$  of kuratite are also apparent in Figure 5. The presence of these apparently strong reflections in the high-order zone-axis patterns are in accordance with X-ray diffraction data of makarochkinite,  $(\text{Ca}_2\text{Fe}^{2+}_4\text{Fe}^{3+}\text{TiSi}_4\text{BeAlO}_{20})$ , which has a composition very similar to kuratite except for the presence of Be (Grew *et al.*, 2005). Unit cell data are given below.

## 2013-109 KURATITE

Triclinic	Space group: $P\bar{1}$ (by analogy to rhönite)	
$a = 10.513 \pm 0.007$	$b = 10.887 \pm 0.007$	$c = 9.004 \pm 0.018 \text{ \AA}$
$\alpha = 105.97 \pm 0.13$	$\beta = 96.00 \pm 0.12$	$\gamma = 124.82 \pm 0.04^\circ$
$V = 767 \pm 2 \text{ \AA}^3$	$Z = 2$	

X-ray powder-diffraction data are not available. Measured  $d$  spacings from TEM SAED patterns are listed in Table 2. The 8 strong reflections in electron diffraction, as determined from high-order zone electron diffraction patterns of sections FIB-1 and FIB-2, are (in the order of decreasing  $d$  spacing):  $03\bar{1}$  (49),  $\bar{2}4\bar{1}$  (78),  $20\bar{3}$  (78),  $4\bar{2}0$  (83),  $21\bar{3}$  (70),  $22\bar{1}$  (32),  $\bar{2}5\bar{1}$  (78) and  $\bar{4}1\bar{1}$  (79); intensities of the corresponding reflections of makarochkinite are given in parentheses. (American Mineralogist Crystal Database, database code amcsd 0003889).

### Crystal structure

The structure could not be determined directly because of the minute size of the crystals.

### Morphology

Habit: euhedral to anhedral grains

Forms:  $\{0\bar{1}1\}$ ,  $\{0\bar{2}1\}$ ,  $\{0\bar{3}1\}$  and others

Twinning: by rotation  $\perp (0\bar{1}1)$ ; polysynthetic

The  $a:b:c$  ratio calculated from the unit cell parameters is 0.966:1:0.827

### NAME

The name is in honour of Professor Dr. Gero Kurat (1938 - 2009), former Head of the Mineralogical-Petrographical Department and Curator of the Meteorite Collection at the Natural History Museum in Vienna, Austria. He was a pioneer in meteorite research and a gifted mineralogist and petrologist. He identified the unusual D'Orbigny meteorite as an angrite.

### TYPE MATERIAL

Holotype kuratite in a rock slab is housed in the collections of the Naturhistorisches Museum Wien, Vienna, Austria, inventory number Section D'Orbigny C-N1172-NH Wien.

### RELATION TO OTHER SPECIES

Although it's not possible to determine the structure of kuratite due to its minute crystal size, the close similarity in crystal chemistry, unit cell type and parameters between kuratite and aenigmatite-rhönite group minerals indicates that kuratite belongs to the aenigmatite-rhönite mineral group. The presence of dominant  $\text{Fe}^{2+}$  in octahedral sites warrants its status as a new mineral (Nickel and Grice, 1998). In this regard, it is interesting to note that Grew *et al.* (2008) pointed out that the mineral  $\text{Ca}_2(\text{Fe}^{2+}_5\text{Ti})(\text{Si}_4\text{Al}_2)\text{O}_{20}$  is the unnamed  $\text{Fe}^{2+}$  analogue of rhönite.

Rhönite is the only aenigmatite-rhönite group minerals reported to include compositions with  $\text{Mg}^{2+}/(\text{Mg}^{2+}+\text{Fe}^{2+}) < 0.5$  and  $\text{Mg}^{2+}/(\text{Mg}^{2+}+\text{Fe}^{2+}) > 0.5$ . Recalculations gave  $\text{Mg}^{2+}/(\text{Mg}^{2+}+\text{Fe}^{2+}) = 0.156-0.499$  for several terrestrial rhönites (Grew *et al.*, 2008 and references therein; Grapes and Keller, 2010), and  $\text{Mg}^{2+}/(\text{Mg}^{2+}+\text{Fe}^{2+}) = 0.17$  and  $0.03$ , respectively, for "rhönite" from Northwest Africa 4590 angrite (Kuehner and Irving, 2007) and Luna 24 regolith (Treiman, 2008). These so-called "rhönites" with  $\text{Mg}^{2+}/(\text{Mg}^{2+}+\text{Fe}^{2+}) < 0.5$  could be categorized into a new kuratite subgroup with the characteristic end-member composition  $\text{Ca}_4(\text{Fe}^{2+}_{10}\text{Ti}_2)\text{O}_4[\text{Si}_8\text{Al}_4\text{O}_{36}]$ .

### UNNAMED MINERAL

**2013-109**  
**KURATITE**

$\text{Ca}_4(\text{Fe}^{2+}_{10}\text{Ti}_2)\text{O}_4[\text{Si}_8\text{Al}_4\text{O}_{36}]$  is currently listed as a valid unnamed mineral with IMA code UM1972-18-SiO:AlCaFeMgTi (Smith and Nickel, 2007, and updates).

**COMPATIBILITY**

Compatibility could not be calculated.

**REFERENCES**

- Anthony, J.W., Bideaux, R.A., Bladh, K.W. and Nichols, M.C. (1995) *Handbook of Mineralogy. Volume II. Silica, Silicates. Part 2.* Mineral Data Publishing, Tucson.
- Ariskin, A.A., Petaev, M.I., Borisov, A.A. and Barmina G.S. (1997) METEOMOD: a numerical model for the calculation of melting-crystallization relationships in meteoritic igneous systems. *Meteoritics and Planetary Science*, **32**, 123-133.
- Bonaccorsi, E., Merlino, S. and Pasero, M. (1990) Rhönite: structural and microstructural features, crystal chemistry and polysomatic relationships. *European Journal of Mineralogy*, **2**, 203-218.
- Grapes, R., and Keller, J. (2010)  $\text{Fe}^{2+}$ -dominant rhönite in undersaturated alkaline basaltic rocks, Kaiserstuhl volcanic complex, Upper Rhine Graben, SW Germany. *European Journal of Mineralogy*, **22**, 285-292.
- Grew, E.S., Barbier, J., Britten, J., Yates, M.G., Polyakov, V.O., Shcherbakova, E.P., Hälenius, U. and Shearer, C.K. (2005) Makarochkinitite,  $\text{Ca}_2\text{Fe}^{2+}_4\text{Fe}^{3+}\text{TiSi}_4\text{BeAlO}_{20}$ , a new beryllosilicate member of the aenigmatite-sapphirine-surinamite group from the Il'men Mountains (southern Urals), Russia. *American Mineralogist*, **90**, 1402-1412.
- Grew, E.S., Hälenius, U., Pasero, M. and Barbier, J. (2008) Recommended nomenclature for the sapphirine and surinamite groups (sapphirine supergroup). *Mineralogical Magazine*, **72**, 839-876.
- Grünhagen, H and Seek, H.A. (1972) Rhönite aus einem Metaphonolith vom Puy de Saint-Sandoux (Auvergne). *Tschermaks Mineralogische und Petrographische Mitteilungen*, **18**, 17-38.
- Jambon, A. and Boudouma, O. (2011) Evidence for rhonite in angrites D'Orbigny and Sahara 99555 (abstract). *Meteoritics and Planetary Science*, **46 Sup.**, A113.
- Kuehner, S.M. and Irving, A.J. (2007) Primary ferric iron-bearing rhönite in plutonic igneous 232 angrite NWA 4590: implications for redox conditions on the angrite parent body. *Eos, AGU*, **88**, Fall Meeting Supplement, Abstract P41A-0219.
- Kunzmann, T. (1999) The aenigmatite-rhönite mineral group. *European Journal of Mineralogy*, **11**, 743-756.
- Kurat, G., Varela, M.E., Brandstätter, F., Weckwerth, G., Clayton, R., Weber, H.W., Schultz, L., Wäsch, E. and Nazarov M.A. (2004) D'Orbigny: A non-igneous angritic achondrite? *Geochimica et Cosmochimica Acta*, **68**, 1901-1921.
- Mittlefehldt, D.W., Killgore, M. and Lee, M.T. (2002) Petrology and geochemistry of D'Orbigny, geochemistry of Sahara 99555, and the origins of angrites. *Meteoritics and Planetary Science*, **37**, 345-369.
- Mukhopadhyay, D.K. and Lindsley, D.H. (1983) Phase relations in the join kirschsteinite ( $\text{CaFeSiO}_4$ )-fayalite ( $\text{Fe}_2\text{SiO}_4$ ). *American Mineralogist*, **68**, 1089-1094.
- Nickel, E.H. and Grice, J.D. (1998) The IMA Commission on New Minerals and Mineral Names: procedures and guidelines on mineral nomenclature. *Canadian Mineralogist*, **36**, 913-926.
- Olsson, H. B. (1983) Rhönite from Skåne (Scania), southern Sweden. *Geologiska Föreningen i Stockholm Förhandlingar*, **105**, 281-286.
- Prinz M. and Weisberg M. K. (1995) Asuka 881371 and the angrites: origin in an heterogeneous, CAI-enriched, differentiated, volatile-depleted body. *Antarctic Meteorites*, **20**, 207-210.
- Smith, D.G.W. and Nickel, E.H. (2007) A system for codification for unnamed minerals: report of the Subcommittee for Unnamed Minerals of the IMA Commission on New Minerals, Nomenclature and Classification. *Canadian Mineralogist*, **45**, 983-1055.

- Treiman, A.H. (2008) Rhönite in Luna 24 pyroxenes: first find from the Moon, and implications for volatiles in planetary magmas. *American Mineralogist*, **93**, 488-491.
- Varela, M.E., Kurat, G., Zinner, E., Métrich, N., Brandstätter, F., Natflos, T. and Sylvester, P. (2003) Glasses in the D'Orbigny angrite. *Geochimica et Cosmochimica Acta*, **67**, 5027-5046.

## AUTHORS' REMARKS

### Sample characterisation

According to SEM BSE observations, besides hollow shells and open vesicles of various sizes and shapes with/without glass filling, D'Orbigny angrite section C has the following silicate phase assemblage: tabular crystals of nearly pure anorthite (An), euhedral to anhedral augite (Aug) crystals with Mg-free and Al-bearing hedenbergite (Hd) rims, euhedral to anhedral olivine (Ol) crystals with Mg-rich cores (Mg ~64 mol%) and complex overgrowths of layers with Mg decreasing and Fe and Ca increasing toward the rim (Figure 1a) (Mittlefehldt *et al.*, 2002). The whole microstructure could be characteristically described as olivine + augite aggregates with highly irregular, brittle fracture-like outlines (as circled in Figure 1a) surrounded by anorthite crystals. Within the olivine + augite aggregates, there is a common presence of multiple phase grain boundary pockets with an overall brighter contrast in SEM-BSE due to Fe sulfides and ulvöspinel (Figure 1a,b). Detailed SEM indicates that the multiple phase pockets sit mainly at olivine-augite triple junctions, and consist of Fe sulfide spherules and euhedral ulvöspinel, fibrous, Na-bearing anorthite, and fibrous whitlockite (Wht), which was described as Ca-phosphate (Mittlefehldt *et al.*, 2002; Kurat *et al.*, 2004), kuratite (Ku), which was described as Ti-silicate or rhönite (Mittlefehldt *et al.*, 2002; Kurat *et al.*, 2004; Jambon and Boudouma, 2011), as well as space-filling Al-bearing hedenbergite (Figure 1).

For the purpose of microstructure analysis, two TEM samples of dimensions 5 µm x 5 µm x 100 nm were prepared by the focused-ion-beam technique from two kuratite grains (inserts in Figure 1d,e). A JEOL 3010 analytical electron microscopy was used for imaging and EDs analyses. Selected area electron diffraction patterns of kuratite and inclusions were taken at various tilt angles for phase identification. A representative TEM bright field micrograph showing a kuratite crystal with abundant polysynthetic nano-twins and whitlockite inclusions in thin section FIB-1 is shown in Figure 3a. Surrounding Fa + Kir intergrowths can also be clearly seen. The twin plane is (0 $\bar{1}1$ ), similar to that reported for other aenigmatite-rhönite group minerals. In contrast, the kuratite crystal in thin section FIB-2 is twin-free and inclusion-free, and is associated with euhedral whitlockite and a rounded Fe sulfide droplet within a polycrystalline herdenbergite matrix (Figure 3b). Kuratite is faceted by small faces, such as (0 $\bar{1}1$ ), (0 $\bar{2}1$ ), (0 $\bar{3}1$ ) *etc.*, as indicated in Figure 3c.

### Origin of the mineral

The crystallization sequence for the phase assemblage of angrites can be deduced from their textures. If the olivine and spinel megacrysts are indeed xenocrysts (*e.g.*, Prinz and Weisberg, 1995; Mittlefehldt *et al.*, 2002) then the crystallization sequence is anorthite + olivine → anorthite + olivine + augite → anorthite + olivine + augite + ulvöspinel (Mittlefehldt *et al.*, 2002). However, modelling the crystallization of the D'Orbigny angrite from its bulk chemical composition following the procedure of Ariskin *et al.* (1997) combined with major and trace element analyses of the compact and porous part of this rock does not support this sequence of crystallization (Kurat *et al.*, 2004). Microstructural characteristics (Figure 6) could be satisfactorily rationalized by the following formation sequences.

1. Original formation of a precursor, porous Ol-Kir-Aug assemblage with multiple-phase grain boundary assemblage (MA) of void + Fe sulfide + Usp in polycrystalline Hd matrix, as shown in Figure 1a. The Hd crystallized as a polycrystalline matrix (Figure 3b), rather than an epitaxial

**2013-109**  
**KURATITE**

rim, around the euhedral augite single crystal, during a late and fast cooling-solidification event. The Ca-rich olivine (Ca ~20 mol.%) and kirschsteinite (Ca ~40 mol.%) as overgrowths on Mg-rich olivine (Figure 1b) is incompatible with retrograde formation of anorthite, the former being stable only under very low Si activity (Prinz and Weisberg, 1995). The exclusive presence of MA at olivine-augite grain triple junctions, but rarely along olivine-anorthite or augite-anorthite grain boundaries, also support the suggestion that Ol-Kir-Aug-MA assemblages predate anorthite.

2. Brittle fracture of the precursor Ol-Kir-Aug-MA assemblage to form fractured fragments with highly irregular outline (Figure 1a).

3. Formation of An plates within/surrounding the porous Ol-Kirs-Aug fragment aggregate.

The occurrence of kuratite + whitlockite within the olivine intergrowths at the contact between Fe sulfide spherules and hedenbergite (Figure 1d, e) suggests that kuratite + whitlockite most likely crystallized very late, near the end of stage 1, together with Fe sulfide spherules and Usp, at Ol-Aug grain triple junctions. This interstitial liquid was Mg-free but enriched in Al-Si-P-Ca-Ti-Fe, and therefore crystallized as Ku + Wht + Fa + Kir + Hd, as observed. The crystallization temperature was probably >1000°C, considering the co-presence of Ca-rich fayalite and kirschsteinite (Mukhopadhyay and Lindsley, 1983) and the 900-1100°C stability field of rhönites based on experimental results (Kunzmann, 1999).

**CHAIRMAN'S REMARKS**

Nil